Available online at www.sciencedirect.com
ScienceDirect
Journal of Catalysis 250 (2007) 264–273
JOURNAL OF CATALYSIS
www.elsevier.com/locate/jcat

Selective oxidation of glycerol over carbon-supported AuPd catalysts

William C. Ketchie [a], Mitsuhiro Murayama [b], Robert J. Davis [a,*]

[a] *Department of Chemical Engineering, University of Virginia, 102 Engineers' Way, PO Box 400741, Charlottesville, VA 22904-4741, USA*
[b] *Department of Materials Science & Engineering, University of Virginia, 116 Engineers' Way, PO Box 400745, Charlottesville, VA 22904-4745, USA*

Received 21 March 2007; revised 11 June 2007; accepted 13 June 2007

Available online 27 July 2007

Abstract

Carbon-supported AuPd bimetallic nanoparticles were synthesized, characterized, and evaluated as catalysts in the aqueous-phase selective oxidation of glycerol. The bimetallic catalysts were synthesized by two different methods. The first method involved the deposition of Au onto the surface of 3-nm supported Pd particles by catalytic reduction of $HAuCl_4$ in aqueous solution by H_2. The second method used the formation of a AuPd sol that was subsequently deposited onto a carbon support. Characterization of the catalysts using analytical transmission electron microscopy, H_2 titration, and X-ray absorption spectroscopy at the Au L_{III} and Pd *K*-edges confirmed that the first synthesis method successfully deposited Au onto the Pd particles. Results from the AuPd sol catalyst also revealed that Au was preferentially located on the surface. Measurement of glycerol oxidation rates (0.3 M glycerol, 0.6 M NaOH, 10 atm O_2, 333 K) in a semibatch reactor gave a turnover frequency (TOF) of 17 s^{-1} for monometallic Au and 1 s^{-1} for monometallic Pd, with Pd exhibiting a higher selectivity to glyceric acid. Although the activity of the bimetallic AuPd catalysts depended on the amount of Au present, none of them had a TOF greater than that of the monometallic Au catalyst. However, the AuPd catalysts had higher selectivity to glyceric acid compared with the monometallic Au. Because a physical mixture of monometallic Au and Pd catalysts also gave higher selectivity to glyceric acid, the Pd is proposed to catalyze the decomposition of the side product H_2O_2 that is also formed over the Au but is detrimental to the selectivity toward glyceric acid.

Keywords: Gold; Palladium; AuPd bimetallic; Hydrogen peroxide; X-ray absorption spectroscopy; Electron microscopy; Glycerol; Glyceric acid; Oxidation; Activated carbon

1. Introduction

Interest in gold catalysis continues to grow, with the recently published review by Hashmi et al. [1] and the book by Bond et al. [2] summarizing the major findings in this area. The low-temperature oxidation of CO over supported Au is the focus of many previous investigations and the general consensus is that Au particles in the range of 2–4 nm are the most active [2]. In many cases, adding water vapor to the feed increases the CO oxidation rates over Au catalysts [3–6]. Furthermore, the use of supported Au catalysts with large particles in the aqueous phase gives high activity in CO oxidation, even though the catalysts are essentially inactive for CO oxidation in the vapor phase [7–9]. The rate of CO oxidation over Au metal particles in aqueous solution depends strongly on pH, with high rates favored at high pH. Interestingly, peroxide formation also occurs during CO oxidation in liquid water [7,8]. Indeed, Au catalysts are also active in the direct synthesis of H_2O_2 from H_2 and O_2 [10,11].

Gold catalysts operating in the aqueous phase also have been shown to be highly active for the oxidation of various alcohols [12–14] and, in particular, glycerol [7,15–17]. Conversion of glycerol is of interest because it is a byproduct of biodiesel production from plant and animal oils [18]. A major surplus of glycerol has resulted from rapid expansion of biodiesel production capacity around the world [19]. The oxidation of glycerol over Au catalysts is one possible route for using this bio-renewable feedstock.

It is well known that bimetallic catalysts can have markedly different activity and selectivity compared with the monometallic analogues [20]. Recently, bimetallic catalysts of Au and Pd exhibited very high alcohol oxidation rates and selectivities in

* Corresponding author. Fax: +1 434 982 2658.
E-mail addresses: wck3z@virginia.edu (W.C. Ketchie), mm2te@virginia.edu (M. Murayama), rjd4f@virginia.edu (R.J. Davis).

0021-9517/$ – see front matter
doi:10.1016/j.jcat.2007.06.011

both solvent-free [21] and aqueous-phase reactions [22–26]. For the solvent-free oxidation of a range of primary alcohols over a titania-supported AuPd bimetallic catalyst, a turnover frequency (TOF) as high as 269,000 h^{-1} at 433 K has been reported [21]. Moreover, the aqueous-phase oxidation of glycerol over AuPd particles supported on activated carbon gave a TOF of 6435 h^{-1} at 323 K, which was 7 times more active and 9% more selective than the monometallic Au catalyst investigated in that study [26].

In the present work, we prepared carbon-supported AuPd bimetallic catalysts synthesized by two different methods; characterized the samples by analytical transmission electron microscopy, H_2 titration, and X-ray absorption spectroscopy; and evaluated their activity and selectivity in the aqueous-phase oxidation of glycerol.

2. Experimental

2.1. Catalyst synthesis

A 3 wt% Pd on activated carbon (Aldrich, lot. 04602PI) was used as received for glycerol oxidation and is designated the Pd catalyst. The Pd catalyst was also used as the precursor for preparing a series of Au on Pd bimetallic catalysts via a redox method [27]. First, 6 g of the Pd catalyst was placed in a glass reactor with 100 cm^3 of distilled deionized water and stirred. The reactor was then purged with N_2 (all gases ultra-high purity [99.999%], provided by Messer Gas) for 30 min. A dihydrogen flow at 100 $cm^3\,min^{-1}$ was bubbled through the slurry while heating to 353 K and holding at that temperature for 1 h. With H_2 continuing to bubble, the reactor was cooled to 298 K, and the pH of the solution was adjusted to 10 by the addition of 1 M NaOH. Next, the appropriate amount of Au, in the form of $HAuCl_4{\cdot}3H_2O$ (Aldrich), was dissolved in 5 cm^3 of distilled deionized water. The gold chloride solution was then added dropwise to the slurry together with the addition of 1 M NaOH to maintain the pH of the slurry near 10. After the addition of gold, the slurry was stirred for 1 h, after which the H_2 flow was stopped and N_2 was used to purge the reactor. The catalyst was filtered and washed twice with 1 L of distilled deionized water to remove residual chlorine. The final filtrate tested negative for Cl^- using a 0.1 M $AgNO_3$ solution. Four catalysts with increasing Au loadings, designated AuPd-A, AuPd-B, AuPd-C, and AuPd-D, were prepared in this manner.

Another AuPd catalyst supported on carbon was prepared through the formation of a gold and palladium bimetallic sol and subsequent deposition of the sol onto the catalyst support. First, 0.091 g of $PdCl_2$ (Aldrich) was added to 0.5 L of distilled deionized water, to which 0.206 g of $HAuCl_4{\cdot}3H_2O$ was then added. Next, 0.154 g of polyvinyl alcohol (PVA; Acros) was added to the solution under vigorous stirring. The AuPd colloid was subsequently reduced by the dropwise addition of 0.1 M $NaBH_4$ (Aldrich), at a $NaBH_4$:metal molar ratio of 4:1. The resulting sol was purple-brown in color. Then 5 g of the catalyst support, activated carbon (Calgon, type ADP), was suspended in 100 cm^3 of distilled deionized water and sonicated for 1 h before being added to the AuPd sol. The sol–carbon slurry was stirred for 1 h and then filtered. The filtrate was clear, indicating that most of the sol had deposited onto the carbon support. The catalyst was then washed twice with 1 L of distilled deionized water to remove residual chlorine. The final filtrate tested negative for Cl^- using a 0.1 M $AgNO_3$ solution. This catalyst is designated AuPd(sol).

A monometallic Au catalyst supported on activated carbon catalyst has been prepared via the gold sol method [28] and fully characterized [7]. First, 0.15 g of $HAuCl_4{\cdot}3H_2O$ (Aldrich) was added to 3 L of distilled deionized water, followed by the addition of 0.075 g of polyvinyl alcohol (PVA; Acros). The gold colloid was subsequently reduced by the dropwise addition of 0.1 M $NaBH_4$ (Aldrich), at a $NaBH_4$:Au molar ratio of 4:1. The resulting sol was ruby-red in color. Then 10 g of activated carbon (Calgon, type ADP) was suspended in 100 cm^3 of distilled deionized water and sonicated for 1 h before being added to the Au sol. The sol–carbon slurry was stirred for 1 h, after which the catalyst was filtered. The filtrate had a slight red tint, indicating that some of the Au sol remained in solution. The catalyst was then washed twice with 1 L of distilled deionized water to remove residual chlorine. The final filtrate tested negative for Cl^- using a 0.1 M $AgNO_3$ solution. The catalyst is designated the Au catalyst.

After preparation, the catalysts were dried overnight in air at 403 K, then reduced in N_2 and H_2 (90:10) flowing at 150 $cm^3\,min^{-1}$ by heating to 573 K at a rate of 4 $K\,min^{-1}$ and holding at 573 K for 6 h. The catalysts were then cooled to room temperature, exposed to air, and stored in a refrigerator at 278 K. The Au and Pd weight loadings were determined by ICP analysis (Galbraith Laboratories, Knoxville, TN).

2.2. Transmission electron microscopy

Samples that were characterized by transmission electron microscopy (TEM) were first suspended in ethanol and agitated in an ultrasonic bath for 4 h. A drop of the suspended catalyst was applied to a copper mesh grid with lacy carbon film, and the ethanol was allowed to evaporate. Microscopy was performed on a JEOL 2010F transmission electron microscope operating at 200 kV and equipped with a Gatan imaging filter (GIF). All images were recorded using a slow-scan CCD camera and analyzed with the Gatan Digital Micrograph software package. Energy-dispersive X-ray spectroscopy (EDS) was done using an Oxford Instruments model 6498 detector and NIST Desktop Spectrum Analyzer software [29]. For analysis of individual particles, the electron beam was focused to a diameter slightly smaller than the diameter of the particle under investigation.

2.3. H_2 titration

Dihydrogen titration of Pd [30] was performed using a Micromeritics ASAP 2020 automated adsorption system. Samples had been stored in atmospheric conditions before H_2 titration of the Pd surface according to the reaction $Pd_sO + 3/2H_2 \rightarrow Pd_sH + H_2O$. The catalysts were evacuated, heated from room temperature to 473 K at a rate of 4 $K\,min^{-1}$, and then held in

vacuum at 473 K for 2 h. H_2 titration was done at 373 K in a pressure range of 0.06–0.6 atm to avoid formation of the β-phase hydride [30]. The surface Pd was evaluated by the total amount of H_2 adsorbed at 373 K extrapolated to zero pressure and dividing by 3 (see stoichiometry above).

2.4. X-ray absorption spectroscopy

X-ray absorption spectroscopy (XAS) was performed at the National Synchrotron Light Source, Brookhaven National Laboratory. The storage ring operated at 2.8 GeV with a ring current of 150–300 mA. Data were collected on beamlines X-10C and X-18B operating in transmission mode at the Pd K-edge (24.350 keV) with a beam spot size of 0.5 mm × 10 mm and at the Au L_{III}-edge (11.919 keV) with a spot size of 1 mm × 10 mm.

Samples were initially pressed into a copper holder and analyzed at ambient conditions. The monometallic Pd sample was also characterized in a sample cell that allowed for heating to 473 K at 4 K min^{-1} under flowing H_2 (g). After 2 h at 473 K, the Pd sample was cooled to 298 K under flowing H_2 (g). For all of the samples, a minimum of 3 scans were collected at 298 K over the appropriate energy range. A second in situ sample cell with its attached flow system (described in Ref. [31]) was also used to analyze various catalysts during aqueous treatment. The samples were placed into a 1.5 mm × 20 mm × 6 mm (X-ray path length) sample holder that was then sealed with poly-ether-ether-ketone (PEEK) disk windows on both sides to allow for the transmission of photons. The cell allowed for data collection while an aqueous solution saturated with 10 atm O_2 was pumped through a packed catalyst bed while heating to 333 K. The flow system consisted of a vessel filled with 60 cm^3 of 0.3 M glycerol and 0.6 M NaOH aqueous solution that was first purged by N_2. Either the N_2 or O_2 saturated solution (10 atm) was then pumped through the packed bed of catalyst at a rate of 1.0 $cm^3\,min^{-1}$ while heating to 333 K. The X-ray scans were collected while the solution flowed through the sample at 333 K.

Analysis of the extended X-ray absorption fine structure (EXAFS) was performed using the WinXAS software package [32]. Between 3 and 6 scans were energy-referenced to either a Pd or Au foil, placed between the transmission and reference ion chambers, then averaged before analysis. The first-shell Pd–Pd amplitude function and phase shift were extracted from a 12.5-μm Pd foil (Goodfellow, 99.95%). The Pd foil was assumed to have the bulk crystallographic values of the Pd fcc structure with a first-shell coordination number (CN) of 12 and nearest-neighbor distance of 2.75 Å. The experimental data were used to optimize the theoretical photoelectron scattering amplitude and phase-shift functions calculated using FEFF8.2 [33]. For analysis of the EXAFS above the Au L_{III}-edge, the energy reference and the first-shell Au–Au amplitude function and phase shift were extracted from a 5-μm Au foil (Goodfellow, 99.9%). The foil was assumed to have the bulk crystallographic values of the Au fcc structure with a first-shell CN of 12 and a nearest-neighbor distance of 2.88 Å, and was used to optimize the theoretically determined amplitude and phase-shift functions calculated by FEFF8.2. The amplitude and phase-shift functions for the heterogeneous absorber–scatterer pairs (Pd–Au and Au–Pd) were also generated using FEFF8.2. For samples evaluated at 298 K, data in the k-range of 3–15 $Å^{-1}$ were used for analysis, whereas for the samples examined under aqueous conditions at 333 K, data in the k-range of 3–14 $Å^{-1}$ were used. Curve fitting was performed in both R-space and k-space with k^1 and k^3 weighting, and the average of these four values is reported herein. The fitting procedure resulted in an estimated accuracy of ±10% for the first-shell CN, ±0.01 Å for interatomic distances, and ±10% for the Debye–Waller factor [34]. The physical constraints necessary for bimetallic fitting set forth by Via et al. [35] were maintained during the fitting process.

2.5. Glycerol oxidation

The aqueous-phase oxidation of glycerol was performed in a 50-cm^3 Parr 4592 batch reactor. The glycerol (Acros) and NaOH (Mallinckrodt) were first dissolved in 30 cm^3 of distilled deionized water and then degassed with He before adding the catalyst. The reactor was then sealed, purged with He, and heated to the desired reaction temperature before pressurizing with O_2. The pressure was maintained at a constant value by continually feeding O_2. Samples were periodically removed using a sample dip tube. The samples from the reaction were filtered (0.2 μm) and then analyzed using a Thermo Separation Products (TSP) Spectra Systems AS1000 high-performance liquid chromatograph (HPLC) equipped with a TSP Spectra Systems P2000 pump and Waters Differential Refractometer model R401. An Aminex HPX-87H column (Bio-Rad) operating at 328 K and a 5 mM H_2SO_4 mobile phase flowing at 0.6 $cm^3\,min^{-1}$ were used for product separation. The retention times and calibration curves for observed products were determined by injecting known concentrations. Any CO_2 that was produced would be converted to Na_2CO_3 in the basic solutions and was quantified by HPLC.

Hydrogen peroxide formed in the reaction mixture was evaluated by a colorimetric method [36]. First, 1 cm^3 of a filtered reaction sample was immediately acidified with 1 cm^3 of 0.5 M H_2SO_4, to which 0.1 cm^3 of $TiO(SO_4)$ (15 wt% in dilute H_2SO_4, Aldrich) was added. Absorbance was then measured at 405 nm on a Varian Cary 3E UV–vis spectrometer. A calibration curve of absorption versus H_2O_2 concentration was prepared by diluting a standard mixture of 30 wt% H_2O_2 (Fisher). The lower limit of H_2O_2 detection is ∼0.005 mM.

3. Results and discussion

Table 1 summarizes the elemental composition, particle size, and hydrogen adsorption capacity of the various catalysts. The particle size determined by TEM was obtained by measuring at least 200 particles over multiple areas for each catalyst. For the series of bimetallic catalysts prepared by Au reduction onto Pd, the average particle size increased with Au loading, which could result from either Au deposition on the surface of the Pd or deposition and growth of monometallic Au particles on the

carbon support. For the AuPd-A, AuPd-B, and AuPd-C samples, the EDS spectra of individual particles revealed particles usually containing both Au and Pd. Fig. 1 shows a representative micrograph along with the EDS spectra for five individual particles of AuPd-B, all of which indicate the presence of both Au and Pd. Although the percentage of monometallic Au particles determined by EDS is low for each of the bimetallic samples prepared by Au deposition onto Pd, the number of monometallic Au particles does in fact increase with Au loading. This is a reasonable observation, because the ability of the Pd to reduce Au with hydrogen will decrease as the Pd is covered with Au.

Dihydrogen titration ($Pd_sO + 3/2H_2 \rightarrow Pd_sH + H_2O$) of the monometallic Pd sample gave a palladium dispersion of 0.33, which is in good agreement with the TEM results indicating a particle size near 3 nm. Interestingly, H_2 titration of the AuPd catalysts prepared by Au deposition revealed Pd dispersions between 0.17 and 0.19 for all four samples. This result is intriguing, because the Au loading on the Pd should significantly depress its H_2 adsorption capacity if the Au were uniformly covering the Pd surface. It is possible that AuPd has a higher hydrogen adsorption capacity than Pd alone [37]. Nevertheless, for all samples prepared by Au deposition onto Pd, some of the Pd appears to be exposed to the surface. In contrast, the sample prepared by the sol method had a Pd dispersion of only 0.01. Because the micrograph of the AuPd(sol) sample (Fig. 2) indicates that the particles are highly dispersed, the Pd appears to be covered by Au. Therefore, the low dispersion value does not appear to be a result of the formation of large Pd crystallites, but rather seems to be due to Au nearly completely covering the Pd surface.

Table 1
Metal weight loadings determined by ICP analysis, particle sizes determined by TEM, and Pd dispersion determined by H_2 titration

Catalyst	Pd (wt%)	Au (wt%)	Atomic ratio Au:Pd	Mean diameter (nm)	Surface average diameter[b] (nm)	H/Pd
Pd	2.9[a]	–	–	2.9	3.3	0.33
Au	–	0.5	–	5.0	7.3	–
AuPd-A	2.9[a]	0.8	0.15	3.2	3.8	0.17
AuPd-B	2.9	1.5	0.28	3.6	4.4	0.19
AuPd-C	2.8[a]	2.2	0.42	3.9	4.4	0.18
AuPd-D	2.8[a]	2.9	0.56	–	–	0.19
AuPd(sol)	0.8	1.1	0.77	3.7	4.8	0.01

[a] Nominal weight loading from the supplier for the monometallic Pd catalyst is 3 wt% Pd, the Pd weight loadings listed are adjusted for the additional Au loading to the parent Pd catalyst based on the Pd ICP results for AuPd-B.
[b] $(\sum d^3)/(\sum d^2)$.

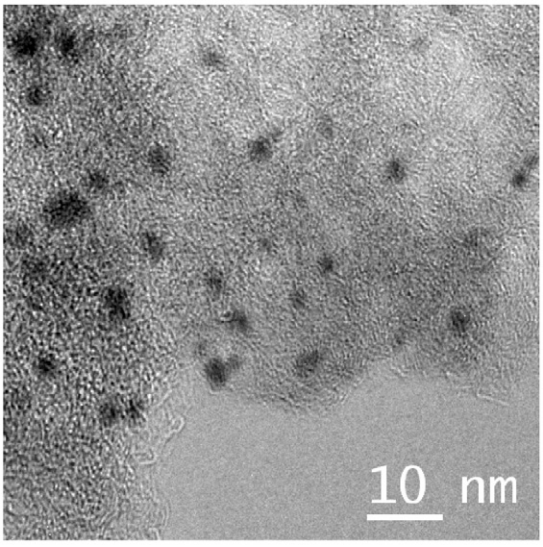

Fig. 2. TEM of AuPd(sol) revealing highly dispersed metal particles.

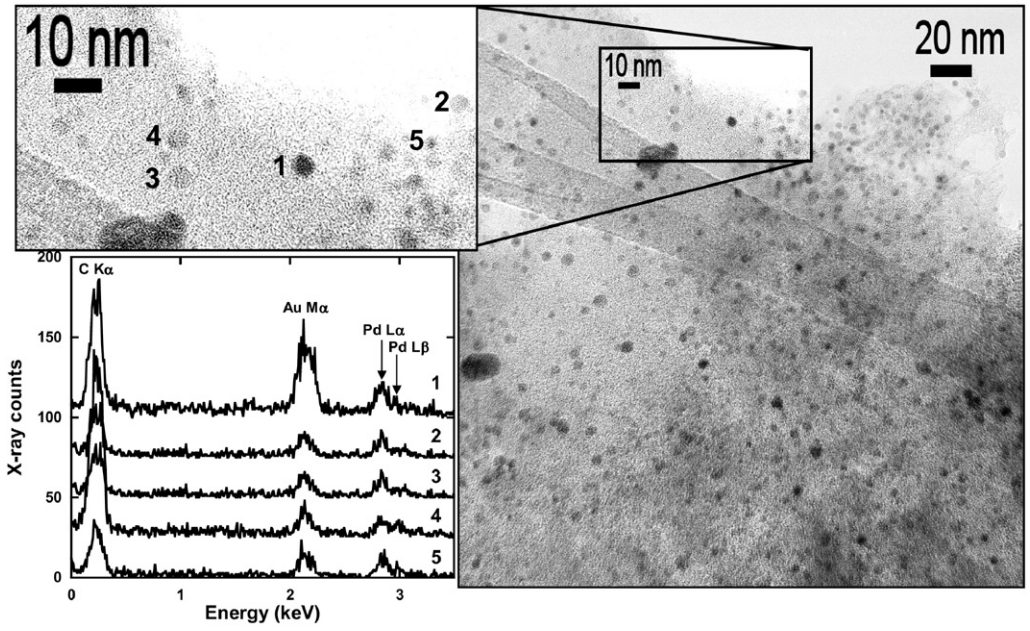

Fig. 1. TEM of sample AuPd-B with EDS spectra of individual particles (numbers correspond to the particle directly to the right of the number). Spectra are offset for clarity.

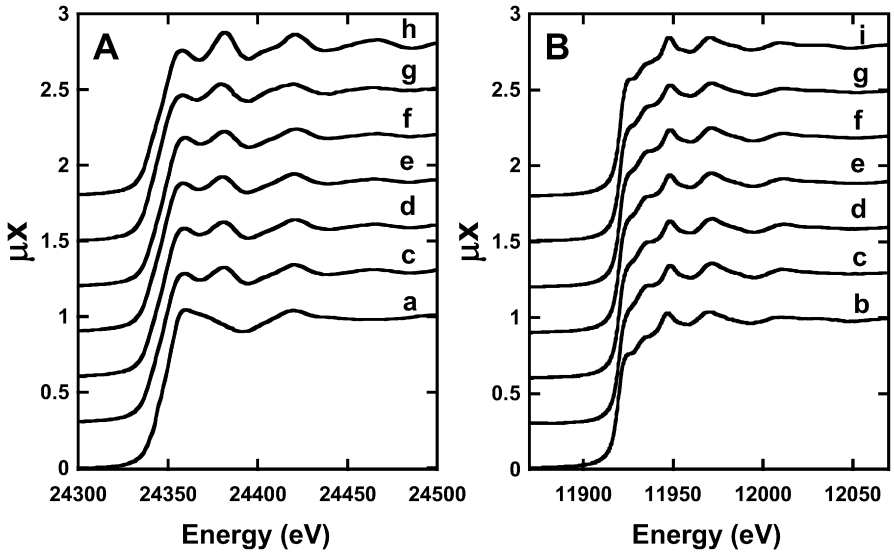

Fig. 3. XANES of the (A) Pd K-edge and (B) Au L_{III}-edge for the samples at ambient conditions, (a) Pd, (b) Au, (c) AuPd-A, (d) AuPd-B, (e) AuPd-C, (f) AuPd-D, (g) AuPd(sol), (h) Pd foil, (i) Au foil. Samples a–g were previously reduced in H_2 at 573 K for 6 h. Spectra are offset for clarity.

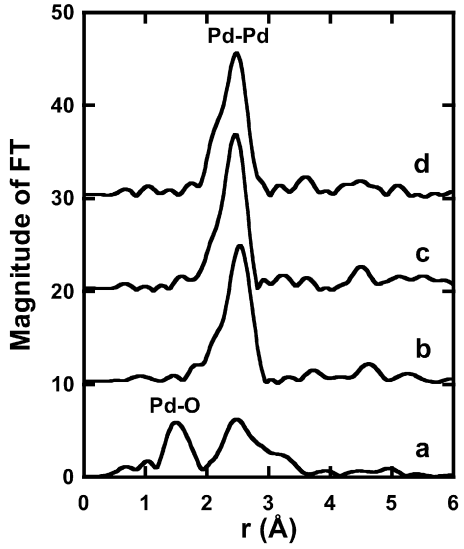

Fig. 4. Fourier transforms (not corrected for phase shifts) of k^3-weighted EXAFS associated with monometallic Pd under various treatments: (a) ambient condition (previously reduced in H_2 at 573 K for 6 h), (b) 1 atm H_2 at 298 K (following 2 h H_2 reduction at 473 K), (c) aqueous treatment for 3 h (0.3 M glycerol, 0.6 M NaOH, N_2 purged, 333 K), (d) aqueous oxidation treatment for 6 h (0.3 M glycerol, 0. 6 M NaOH, 10 atm O_2, 333 K). Spectra are offset for clarity.

Results from X-ray absorption spectroscopy at the Pd K-edge, illustrated in Figs. 3A(a) and 4a, show that the Pd catalyst (which was previously reduced in H_2 at 573 K for 6 h) is highly oxidized on exposure to air. The in situ treatment of Pd in 1 atm H_2 at 473 for 2 h reduces the oxide to Pd metal (Fig. 4b) with EXAFS fitting, indicating an elongation of the first-shell Pd–Pd interatomic distance (Table 2), characteristic of β-phase Pd hydride formation [38]. The oxidized Pd catalyst was also reduced by an aqueous solution of glycerol (0.3 M glycerol, 0.6 M NaOH, 10 atm N_2, 333 K) (Fig. 4c). After the addition of 10 atm O_2 to the glycerol solution and subsequent 6 h treatment (Fig. 4d) at the oxidation reaction conditions, the Pd appeared to remain in the metallic state. Evidently, glycerol is an adequate reductant for maintaining Pd in the metallic state, even under high dioxygen pressure.

The X-ray absorption near-edge structure (XANES) at the Pd K-edge of the AuPd catalysts confirmed that the bimetallic catalysts were in the metallic state even after exposure to air (Fig. 3a). This observation for the series of AuPd catalysts prepared by the redox method is in contrast with that for the parent Pd catalyst, which was readily oxidized by ambient air. The suppression of Pd oxidation by Au is further evidence of the Au–Pd interaction. The XANES at the Au L_{III}-edge for all of the gold-containing catalysts (Fig. 3b) indicated that Au was always present in the metallic state.

Representative χ data with k^3 weighting and Fourier-transformed k^3-weighted χ functions for a bimetallic AuPd sample are presented in Figs. 5 and 6, respectively. The curve fits in R-space are also shown in Fig. 6. The EXAFS fitting results for all of the samples are summarized in Table 2. The first-shell Pd–Pd CN for the Pd catalyst was approximately 9 for both a sample reduced via H_2 (g) and a sample treated under aqueous oxidation conditions, indicating that the Pd particles were stable during aqueous phase conditions. For the series of AuPd(A–D) catalysts prepared from the same parent Pd catalyst, the first-shell Pd–Pd CN was relatively unchanged. However, the spectra revealed small contributions arising from Pd–Au interactions. These results demonstrate that the Pd particles were relatively unaltered by the addition of the Au. The EXAFS analysis of the Au edge clearly shows significant interactions with Pd. The Fourier transform shown in Fig. 6b illustrates the modification of the Au environment in the bimetallic catalyst compared with Au foil. The characterization of AuPd-B under glycerol oxidation conditions revealed little change in the CNs for the various absorber–scatterer pairs compared with the as-prepared catalyst, indicating good stability of the bimetallic

Table 2
Results from EXAFS fitting

Catalyst	Treatment	Absorber–scatterer	1st shell CN	Interatomic distance (Å)	$\Delta\sigma^2$ (Å^2)	ΔE_0 (eV)
Pd	A	Pd–Pd	9.3	2.81	0.0076	−2.6
Pd	B	Pd–Pd	8.7	2.74	0.0069	−3.5
Au	C	Au–Au	10.2	2.84	0.0091	−2.6
AuPd-A	C	Pd–Pd	9.0	2.74	0.0071	2.3
		Pd–Au	0.5	2.77	0.0082	2.3
		Au–Pd	3.5	2.77	0.0082	0.7
		Au–Au	7.7	2.83	0.0085	0.7
AuPd-B	C	Pd–Pd	9.1	2.74	0.0071	−3.2
		Pd–Au	0.7	2.77	0.0066	−3.2
		Au–Pd	2.6	2.77	0.0066	−2.1
		Au–Au	8.3	2.83	0.0088	−2.1
AuPd-B	B	Pd–Pd	8.7	2.75	0.0071	−4.0
		Pd–Au	0.8	2.79	0.0060	−4.0
		Au–Pd	3.0	2.79	0.0060	0.9
		Au–Au	8.2	2.85	0.0074	0.9
AuPd-C	C	Pd–Pd	8.8	2.74	0.0070	−2.0
		Pd–Au	1.0	2.77	0.0074	−2.0
		Au–Pd	2.4	2.77	0.0074	−1.5
		Au–Au	8.7	2.83	0.0079	−1.5
AuPd-D	C	Pd–Pd	8.6	2.74	0.0073	−3.0
		Pd–Au	1.0	2.77	0.0064	−3.0
		Au–Pd	1.9	2.77	0.0064	−0.8
		Au–Au	10.0	2.83	0.0088	−0.8
AuPd(sol)	C	Pd–Pd	6.0	2.75	0.0068	−4.2
		Pd–Au	1.3	2.77	0.012	−4.2
		Au–Pd	1.7	2.77	0.012	−1.3
		Au–Au	10.0	2.83	0.0099	−1.3

Treatments: (A) 1 atm H_2 (g) at 298 K, following reduction at 473 K; (B) aqueous oxidation conditions, 0.3 M glycerol, 0.6 M NaOH, 10 atm O_2, at 333 K; (C) as-prepared in air.

particles in the aqueous phase. However, all of the interatomic distances increased slightly by 0.01–0.02 Å, which may correspond to a relaxation of metal–metal bonds in solution.

Fitting of the Au edge for sample AuPd-A gave a Au–Au first-shell CN of 7.7 and a Au–Pd CN of 3.5, indicating that 31% of all the Au nearest neighbors were Pd. In addition, the Au–Au interatomic distance of 2.83 Å in the bimetallic catalyst was contracted by 0.05 Å compared with that of the bulk, as expected for highly dispersed Au particles [39]. An ideal monolayer of Au on the (111) surface of Pd would have CNs of 6 for Au–Au and 3 for Au–Pd, not too different from our results for AuPd-A. As the Au loading increased, the average Au–Au CN increased while the Au–Pd CN decreased, suggesting that once a maximum loading of Au is deposited onto the Pd, the Au begins to form separate monometallic particles. Thus, results from the Au and Pd EXAFS of the samples prepared by the surface redox method are consistent with the Pd particles remaining intact as Au was deposited onto the Pd. Although some alloying of Au and Pd may have occurred at the Au–Pd interface, the EXAFS results indicate that bulk alloying of the two metals did not occur under our conditions.

The AuPd(sol) was prepared according to the procedure described by Prati et al. [25]. Their catalyst characterization results suggested that both alloyed particles and monometallic Pd particles were present. Results from our EXAFS characterization of the AuPd(sol) catalyst suggest that Au and Pd were not well alloyed. Although the CNs for Pd–M and Au–M interactions indicate that the Pd was more highly dispersed than the Au, the lack of significant H_2 adsorption capacity revealed that the Au was covering the surface of the Pd.

The well-characterized catalysts were then tested in the oxidation of glycerol by O_2. The reaction conditions were typical of those used to study glycerol oxidation [15–17]. To ensure that O_2 mass transfer was not limiting, the maximum O_2 transfer rate for our reactor setup was determined by measuring the oxidation rate of an aqueous solution of Na_2SO_3 to Na_2SO_4 by O_2 [40]. The rate-controlling step in the reaction was assumed to be the mass transfer of O_2 from the vapor phase into the aqueous phase. The oxidation of sodium sulfite at our standard agitation speed and 10 atm O_2 resulted in a maximum transport rate of 6×10^{-6} (mol O_2) s^{-1}. Therefore, catalyst loadings were chosen to ensure that glycerol oxidation rates stayed below this value. The rates of glycerol consumption and H_2O_2 production were based on the first 30 min of reaction. The rate of H_2O_2 production was not corrected for the decomposition reaction; that is, the rate was based on the observed amount of H_2O_2 at 30 min. Selectivity was defined as the total number of moles of species i formed per total number of moles of glycerol converted for the given reaction time. The molar sum of all C_3 and C_2 species was always within 3% of the initial glycerol loading in the reactor, which is within the expected error for HPLC analysis. The C_1 products consisted of carbon dioxide, trapped in solution as Na_2CO_3, and formic acid. Acids were present in their salt forms at the elevated pH.

The two monometallic Pd and Au catalysts were first tested for glycerol oxidation at 0.3 M glycerol, 0.6 M NaOH, 10 atm O_2, and $T = 333$ K. The rates per mol of metal were 0.3 s^{-1} for Pd and 2.4 s^{-1} for Au, corresponding to TOFs of 1 s^{-1} for Pd and 17 s^{-1} for Au after accounting for particle size (Table 3). Thus, Au was significantly more active for oxidation than Pd under the reaction conditions investigated, whereas the Pd catalyst was more selective to glyceric acid than Au. It is also important to note that the Pd catalyst demonstrated a significant drop in activity as the reaction proceeded, reaching only 30% conversion after 5 h.

Table 3 presents the observed rate and selectivity to glyceric acid at 50% conversion for all of the catalysts, and Fig. 7 gives a representative reaction plot of glycerol consumption and product selectivity. For the series of AuPd catalysts prepared by Au deposition, the TOF increased with increasing Au loading, but never reached the maximum TOF observed over monometallic Au. Moreover, the TOF observed on the AuPd(sol) catalyst was very similar to that of the high-loaded AuPd catalysts prepared by Au deposition onto Pd. Because the results from H_2 titration suggest that the surface of the AuPd(sol) catalyst was nearly all Au, the measured TOF is consistent with a pure gold surface and was within a factor of 2.5 of the monometallic Au catalyst. Considering all of these results, it appears that one role of Pd is to help keep Au in a highly dispersed form. However, because the observed TOF never exceeded that of a pure Au catalyst, no synergistic effect of Pd on the activity of Au was observed.

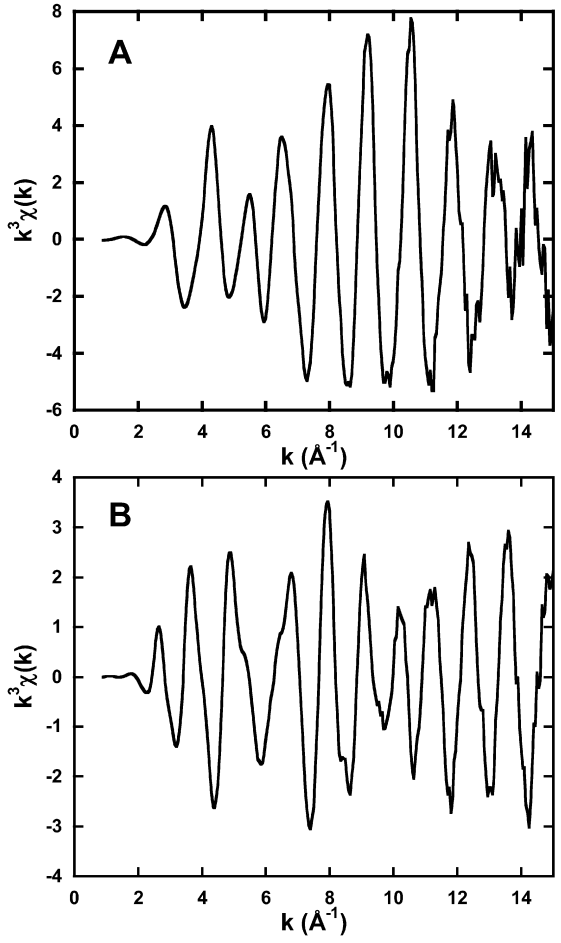

Fig. 5. Experimental χ data with k^3 weighting for AuPd-B; (A) Pd K-edge and (B) Au L_{III}-edge. Spectra were collected at ambient conditions.

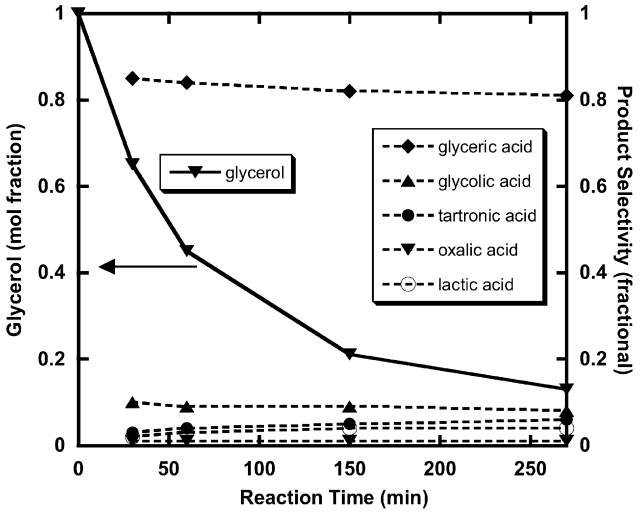

Fig. 7. Glycerol oxidation over AuPd-A. Reaction conditions: 30 cm^3, 0.3 M glycerol, 0.6 M NaOH, glycerol:Au = 50,000:1, $T = 333$ K, $O_2 = 10$ atm.

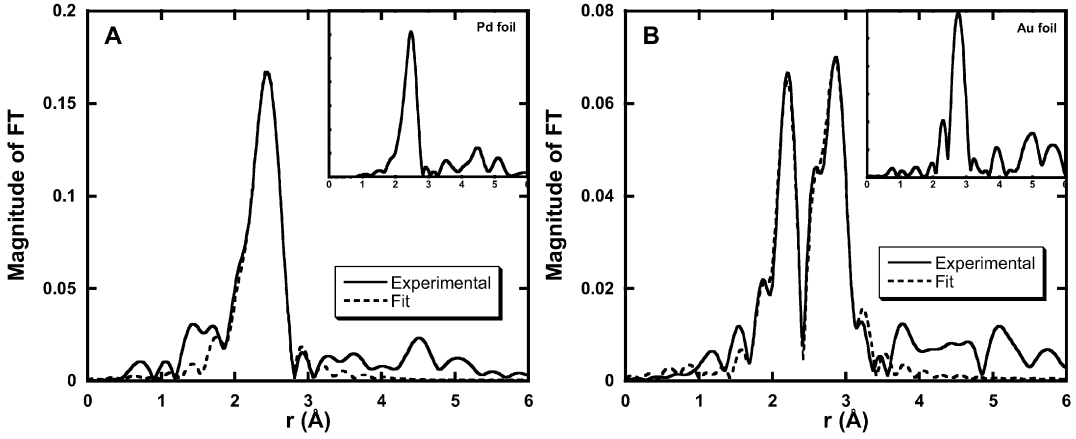

Fig. 6. Magnitude of the Fourier transformed k^3-weighted χ function from Fig. 5 (not corrected for phase shifts) with non-linear least squares fits for sample AuPd-B; (A) Pd (Pd–Pd and Pd–Au shells) and (B) Au (Au–Au and Au–Pd shells). Data were collected at ambient conditions.

Table 3
Initial ($t = 30$ min) glycerol oxidation rates, H_2O_2 formation rates, and selectivity to glyceric acid[a]

Catalyst	Oxidation rate [mol glycerol (mol metal)$^{-1}$ s^{-1}]	Oxidation TOF[b] (s^{-1})	Peroxide rate[c] [mol H_2O_2 (mol metal)$^{-1}$ s^{-1}]	Peroxide TOF[b] (s^{-1})	Sel. to glyceric acid at 50% conv.
Pd	0.3	1.0	<0.0005	–	0.82[d]
Au	2.4	17	0.048	0.34	0.65
AuPd-A	1.2	4.6	0.002	0.008	0.84
AuPd-B	1.3	5.6	0.007	0.030	0.82
AuPd-C	1.6	7.0	0.012	0.052	0.80
AuPd-D	1.4	–	0.010	–	0.80
AuPd(sol)	1.3	6.2	0.042	0.20	0.64
Au & Pd[e]	0.6	2.1	0.001	0.003	0.84
Au & Pd[f]	0.7	2.5	0.002	0.007	0.84

[a] Reaction conditions, 30 cm^3, 0.3 M glycerol, 0.6 M NaOH, 10 atm O_2, 333 K. Catalyst loadings were: glycerol:Pd = 3000 for Pd; glycerol:Au = 50,000:1 for Au, AuPd-A, AuPd-B, AuPd-C, AuPd-D; glycerol:Au = 25,000 for AuPd(sol).
[b] Rates normalized for surface atoms using the inverse of the surface avg. diameter from Table 1.
[c] Rates of H_2O_2 formation have not been corrected for decomposition/consumption.
[d] Pd sample appeared to suffer from deactivation, selectivity given at 30% conversion ($t = 5$ h).
[e] Physical mixture of monometallic Au and Pd (glycerol:Au = 50,000:1 and glycerol:Pd = 3000:1).
[f] Physical mixture of monometallic Au and Pd (glycerol:Au = 50,000:1 and glycerol:Pd = 7000:1).

In contrast to our findings related to catalyst activity, the presence of Pd appeared to improve the selectivity toward glyceric acid. Table 3 shows a corresponding decrease in H_2O_2 production with the observed increase in selectivity over the bimetallic catalysts prepared by Au deposition. In our previous work [7] we proposed that H_2O_2 formed in situ over Au catalysts is responsible for the observed C–C cleavage that led to the major C_2 product glycolic acid (Scheme 1). Therefore, our results with the Au–Pd series are completely consistent with decreasing H_2O_2 concentration being related to higher selectivity to glyceric acid.

To test whether the decomposition of H_2O_2 in situ results in increased selectivity to glyceric acid, a known peroxide decomposer, MnO_2 [41], was added to the reaction mixture. Approximately 0.3 g of MnO_2 (Aldrich) with a surface area of 1.1 m^2 g^{-1} was added to a standard glycerol oxidation reaction (30 cm^3, 0.3 M glycerol, 0.6 M NaOH, 333 K, 10 atm O_2, and monometallic Au at glycerol:Au = 16,000:1). Although the initial concentration of H_2O_2 was 1.7 mM H_2O_2 in the absence of MnO_2, it was reduced to 0.12 mM with MnO_2. Moreover, the selectivity at 40% glycerol conversion increased from 64 to 78% with addition of MnO_2. These results suggest that decomposing the peroxide formed on Au can significantly increase the selectivity of oxidation reactions. Unfortunately, the addition of MnO_2 decreased the initial glycerol oxidation rate by 50%, possibly indicating that some of the activity observed over Au catalysts is due to the oxidizing ability of the peroxide or the peroxide precursor, superoxide.

To determine whether the Pd decomposes the peroxide produced over Au or whether the formation of AuPd bimetallic catalysts minimizes peroxide formation, a physical mixture of Au and Pd monometallic catalysts was evaluated in glycerol oxidation. As shown in Table 3, the H_2O_2 was decreased on the addition of Pd, resulting in a glyceric acid selectivity of 84% at 50% conversion compared with 64% over Au alone. Because the carbon support of the commercial Pd catalyst is likely different from the Calgon carbon support used for the Au catalyst, a Pd/Calgon carbon catalyst was synthesized in our laboratory to determine whether the observed changes in selectivity can be attributed to the Pd or to the commercial carbon support. The Pd/Calgon catalyst was prepared by incipient wetness impregnation of aqueous $PdCl_2$, followed by washing with water and reduction in flowing H_2 at 573 K for 6 h. This procedure resulted in 1.9 m^2 surface Pd per gram of catalyst, as determined by H_2 titration. Glycerol oxidation with the physical mixture of Au and Pd/Calgon (at the same reaction conditions and equal loadings of surface Pd as in Table 3, entry 8) gave a glycerol oxidation TOF of 1.9 s^{-1}, a peroxide concentration that was below detection at $t = 30$ min, and a selectivity to glyceric acid at 50% conversion of 79%. The results suggest that Pd is responsible for the decomposition of peroxide and the increased selectivity to glyceric acid.

Unlike with the addition of MnO_2, addition of Pd did not decrease the observed rate of glycerol conversion, because the sum of the conversion for the two individual monometallic catalysts (at equivalent loadings) was very similar to that of a physical mixture. The presence of Pd, even if physically separated from the Au, significantly enhances the selectivity to glyceric acid by decomposing the H_2O_2. Therefore, it appears that the small amount of exposed Pd in the series of AuPd catalysts prepared by deposition was responsible for the increased selectivity to glyceric acid. Although both Au and Pd were present in the AuPd(sol) catalyst, there was no observed increase in glyceric acid selectivity compared with monometallic Au, because the Pd was almost completely covered by Au.

4. Conclusion

Two different synthesis methods were used for the preparation of AuPd bimetallic catalysts. The direct deposition of Au onto a parent Pd monometallic catalyst was successful for preparing a series of Au on Pd catalysts. Catalyst characterization using TEM, H_2 titration, and XAS indicated that there may be a maximum Au coverage on the Pd after which additional Au deposited as monometallic clusters on the catalyst

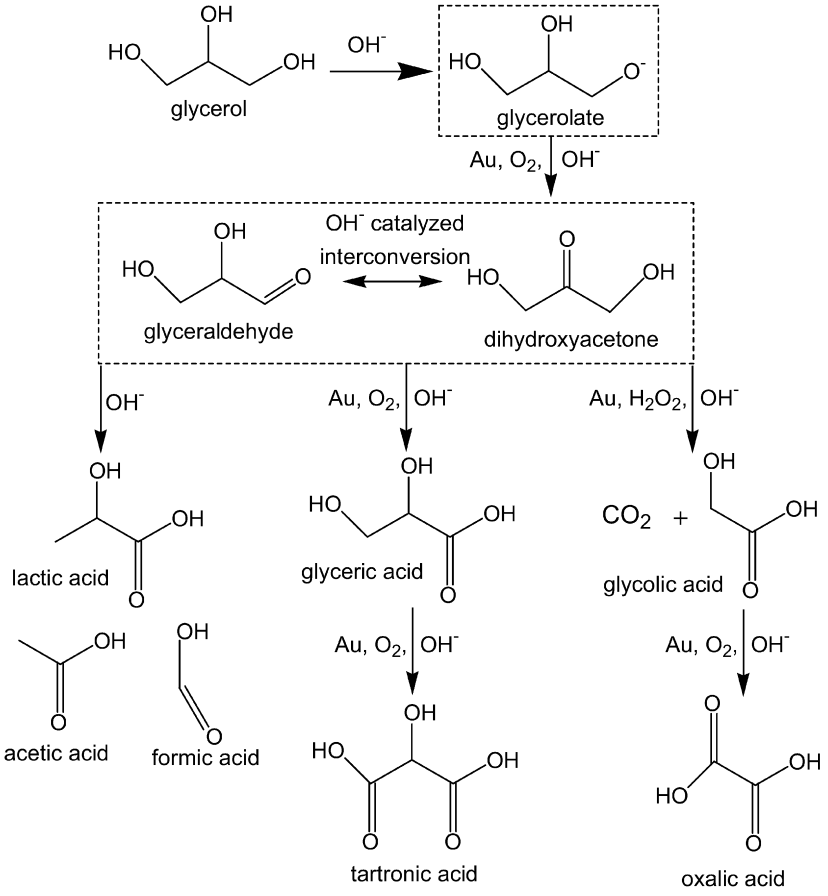

Scheme 1. Proposed reaction network for the aqueous phase oxidation of glycerol over supported Au catalysts in the presence of a strong base. Species within boxes are proposed intermediates that were never directly isolated.

support. Nevertheless, the parent Pd catalyst maintained the Au in a highly dispersed state. In situ XAS characterization of the Pd catalyst and a AuPd bimetallic catalyst revealed good particle stability during aqueous-phase oxidation. Moreover, the Pd and Au appear to be metallic under reaction conditions. The preparation of AuPd sol gave a catalyst in which the Au almost completely covered the Pd.

Results from this study indicate there is not a significant rate enhancement for the bimetallic catalysts compared with monometallic Au after rates have been properly normalized to the surface metal concentration. But there does appear to be an important influence of Pd on the selectivity of the glycerol oxidation reaction. Kinetic studies revealed that Pd in either a bimetallic particle or a physical mixture with Au decreased the amount of observed H_2O_2 in the reaction. Because H_2O_2 is correlated with the formation of C–C cleavage products, the presence of Pd with Au increased the selectivity of the glycerol oxidation reaction to the formation of glyceric acid.

Acknowledgments

This work was supported by the National Science Foundation (Grants CTS-0313484 and CTS-0624608). Research was carried out in part on beamlines X-10C (operated by the Exxon-Mobil Research and Engineering Company) and X-18B (operated by the Synchrotron Catalysis Consortium, which is funded by US Department of Energy Grant DE-FG02-05ER15688) at the National Synchrotron Light Source, Brookhaven National Laboratory, which is supported by the US Department of Energy, Division of Materials Sciences and Division of Chemical Sciences, under Contract DE-AC02-98CH10886. We also acknowledge partial support from the US Department of Energy, Office of Basic Energy Sciences (Grant DE-FG02-95ER14549).

References

[1] A.S.K. Hashmi, G.J. Hutchings, Angew. Chem. Int. Ed. 45 (2006) 7896.
[2] G.C. Bond, C. Louis, D.T. Thompson, Catalysis by Gold, Imperial College Press, London, 2006.
[3] J.T. Calla, R.J. Davis, Ind. Eng. Chem. Res. 44 (2005) 5403.
[4] C.K. Costello, J.H. Yang, Y.W.H.Y. Law, J.N. Lin, L.D. Marks, M.C. Kung, H.H. Kung, Appl. Catal. A 243 (2003) 15.
[5] M. Date, M. Haruta, J. Catal. 201 (2001) 221.
[6] M. Date, M. Okumura, S. Tsubota, M. Haruta, Angew. Chem. Int. Ed. 43 (2004) 2129.
[7] W.C. Ketchie, M. Murayama, R.J. Davis, Top. Catal. 44 (2007) 307.
[8] M.A. Sanchez-Castillo, C. Couto, W.B. Kim, J.A. Dumesic, Angew. Chem. Int. Ed. 43 (2004) 1140.
[9] W.B. Kim, T. Voitl, G.J. Rodriquez-Rivera, J.A. Dumesic, Science 305 (2004) 1280.
[10] M. Okumura, Y. Kitagawa, K. Yamagcuhi, T. Akita, S. Tsubota, M. Haruta, Chem. Lett. 23 (2003) 822.
[11] P. Landon, P.J. Collier, A.F. Carley, D. Chadwick, A.J. Papworth, A. Burrows, C.J. Kiely, G.J. Hutchings, Phys. Chem. Chem. Phys. 5 (2003) 1917.

[12] L. Prati, M. Rossi, J. Catal. 176 (1998) 552.
[13] L. Prati, F. Porta, Appl. Catal. A 291 (2005) 199.
[14] S. Biella, G.L. Castiglioni, C. Fumagalli, L. Prati, M. Rossi, Catal. Today 72 (2002) 43.
[15] S. Carrettin, P. McMorn, P. Johnston, K. Griffin, G.J. Hutchings, Chem. Commun. (2002) 696.
[16] F. Porta, L. Prati, J. Catal. 224 (2004) 397.
[17] S. Demirel-Gulen, M. Lucas, P. Claus, Catal. Today 102–103 (2005) 166.
[18] A.H. Tullo, Chem. Eng. News 85 (2007) 53.
[19] M. McCoy, Chem. Eng. News 84 (2006) 7.
[20] J.H. Sinfelt, Bimetallic Catalysts, Wiley, New York, 1983.
[21] D.I. Enache, J.K. Edwards, P. Landon, B. Solsona-Espriu, A.F. Carley, A.A. Herzing, M. Watanabe, C.J. Kiely, D.W. Knight, G.J. Hutchings, Science 311 (2006) 362.
[22] N. Dimitratos, J.A. Lopez-Sanchez, D. Lennon, F. Porta, L. Prati, A. Villa, Catal. Lett. 108 (2006) 147.
[23] N. Dimitratos, A. Villa, D. Wang, F. Porta, D. Su, L. Prati, J. Catal. 244 (2006) 113.
[24] N. Dimitratos, L. Prati, Gold Bull. 38 (2005) 73.
[25] C.L. Bianchi, P. Canton, N. Dimitratos, F. Porta, L. Prati, Catal. Today 102–103 (2005) 203.
[26] D. Wang, A. Villa, F. Porta, D. Su, L. Prati, Chem. Commun. (2006) 1956.
[27] J. Barbier, P. Marecot, G.D. Angel, P. Bosch, J.P. Boitiaux, B. Didillon, J.M. Dominguez, I. Schifter, G. Espinosa, Appl. Catal. A 116 (1994) 179.
[28] L. Prati, G. Martra, Gold Bull. 32 (1999) 96.
[29] C.E. Fiori, C.R. Swyt, R.L. Myklebust, Desktop Spectrum Analyzer (Program), National Institute of Standards and Technology, Gaithersburg, MD, 1992.
[30] J.E. Benson, H.S. Hwang, M. Boudart, J. Catal. 30 (1973) 146.
[31] E.P. Maris, W.C. Ketchie, V. Oleshko, R.J. Davis, J. Phys. Chem. B 110 (2006) 7869.
[32] T. Ressler, WinXAS, 2.33 ed., Berlin, 2001.
[33] A.L. Aunkudinov, C. Bouldin, J.J. Rehr, J. Sims, H. Hung, Phys. Rev. B 65 (2002) 104107.
[34] D.C. Koningsberger, B.L. Mojet, G.E.v. Dorseen, D.E. Ramaker, Top. Catal. 10 (2000) 143.
[35] G.H. Via, J.K.F. Drake, G. Meitzner, F.W. Lytle, J.H. Sinfelt, Catal. Lett. 5 (1990) 25.
[36] C.N. Satterfield, A.H. Bonnell, Anal. Chem. 27 (1955) 1174.
[37] L. Piccolo, A. Piednoir, J.C. Bertolini, Surf. Sci. 600 (2006) 4211.
[38] R.J. Davis, S.M. Landry, J.A. Horsley, M. Boudart, Phys. Rev. B 39 (1989) 10580.
[39] J.T. Miller, A.J. Kropf, J.R.R.Y. Zha, L. Delannoy, C. Louis, E. Bus, J.A.v. Bokhoven, J. Catal. 240 (2006) 222.
[40] B. Maier, C. Dietrich, J. Buchs, Trans. IChemE 79 (2001) 107.
[41] M.A. Hasan, M.I. Zaki, L. Pasupulety, K. Kumari, Appl. Catal. A 181 (1999) 171.